Two Classes of Gating Current from L-Type Ca Channels in Guinea Pig Ventricular Myocytes

ROMAN SHIROKOV, RICHARD LEVIS, NATALIA SHIROKOVA, and EDUARDO RÍOS

From the Department of Physiology, Rush University, Chicago, Illinois 60612

ABSTRACT Intramembrane charge movement was recorded in guinea pig ventricular myocytes at 19–22°C using the whole-cell patch clamp technique. From a holding potential of −110 mV, the dependence of intramembrane charge moved on test voltage ($Q(V)$) followed the sum of two Boltzmann components. One component had a transition voltage ($\overline{V}$) of −48 mV and a total charge (Q_{max}) of ≃3 nC/μF. The other had a $\overline{V}$ of −18 mV and a Q_{max} of 11 nC/μF. Ba^{2+} currents through Ca channels began to activate at −45 mV and peaked at ≃−15 mV. Na^+ current peaked at −35 to −30 mV. Availability of charge (in pulses from −70 to +10 mV) depended on the voltage of conditioning depolarizations as two Boltzmann terms plus a constant. One term had a $\overline{V}$ of −88 mV and a Q_{max} of 2.5 nC/μF; the other had a $\overline{V}$ of −29 mV and a Q_{max} of 6.3 nC/μF. From the $Q(V)$ dependence, the voltage dependence of the ionic currents, and the voltage dependence of the availability of charge, the low voltage term of $Q(V)$ and availability was identified as Na gating charge, at a total of 3.5 nC/μF. The remainder, 11 nC/μF, was attributed to Ca channels. After pulses to −40 mV and above, the OFF charge movement had a slow exponentially decaying component. Its time constant had a bell-shaped dependence on OFF voltage peaking at 11 ms near −100 mV. Conditioning depolarizations above −40 mV increased the slow component exponentially with the conditioning duration ($\tau \cong 480$ ms). Its magnitude was reduced as the separation between conditioning and test pulses increased ($\tau \cong 160$ ms). The voltage distribution of the slow component of charge was measured after long (5 s) depolarizations. Its $\overline{V}$ was −100 mV, a shift of −80 mV from the value in normally polarized cells. This voltage was the same at which the time constant of the slow component peaked. Q_{max} and the steepness of the voltage distribution were unchanged by depolarization. This indicates that the same molecules that produce the charge movement in normally polarized cells also produce the slow component in depolarized cells. 100 μm D600 increased by 77% the slow charge movement after a 500-ms conditioning pulse. These results demonstrate two classes of charge

Address reprint requests to Dr. Eduardo Ríos, Department of Physiology, Rush University, 1050 W. Harrison St., Chicago, IL 60612.

The permanent address of Roman Shirokov and Natalia Shirokova is A. A. Bogomoletz Institute of Physiology, Acad. Sci. Ukraine, Bogomoletz Str. 4, 252601 GSP, Kiev 24, Ukraine.

J. GEN. PHYSIOL. © The Rockefeller University Press · 0022-1295/92/06/0863/33 $2.00
Volume 99 June 1992 863–895

movement associated with L-type Ca channels, with kinetics and voltage dependence similar to charge 1 and charge 2 of skeletal muscle. The slow component corresponds to charge 2, and probably originates in transitions between inactivated states of the L-type Ca channels.

INTRODUCTION

Studies of intramembrane charge movement have illuminated both the gating of ionic channels in axons (Armstrong and Bezanilla, 1973; Keynes and Rojas, 1974; Armstrong, 1981 for review) and excitation–contraction (E-C) coupling in skeletal muscle (Schneider and Chandler, 1973; reviewed by Ríos and Pizarro, 1991). Asymmetric charge movements have also been described in the nerve cell bodies (Kostyuk, Krishtal, and Pidoplichko, 1977; Adams and Gage, 1979). Intramembrane charge movement has recently been measured in isolated mammalian cardiac myocytes (Field, Hill, and Lamb, 1988; Bean and Ríos, 1989; Hadley and Lederer, 1989, 1991; Hanck, Sheets, and Fozzard, 1990). The voltage dependence of activation and pharmacological and electrophysiological data led to a tentative separation of two components, identified as Na and L-type Ca channel gating currents.

Several previous studies found scattered evidence of effects of voltage-dependent inactivation on both kinetics and voltage dependence of charge movement. In the present work we studied charge movement in guinea pig ventricular myocytes to clarify the effects of voltage-dependent inactivation. To that end we first reevaluated the amount of Na channel gating current by a combination of methods, and concluded that it constitutes $\simeq 25\%$ of the total. This indicates that by far the largest portion of charge movement in these cells arises from the gating of L-type Ca channels.

We then studied the effects of depolarization on charge movement. Depolarizing pulses beyond -30 mV, of 50 ms or longer duration, did not immobilize the charge. Instead, they drastically changed its voltage dependence. These effects were almost identical to those of depolarization on the properties of skeletal muscle charge movement (Brum and Ríos, 1987). The similarity was not unexpected; skeletal muscle charge movement arises mostly at dihydropyridine (DHP)-binding voltage sensors, analogous to the L-type Ca channels that originate most of the charge movement in the guinea pig myocyte. Here, as in skeletal muscle, the effects could be accurately described as the result of an interconversion between two classes of mobile charge: the charge that moves when a resting channel is activated by depolarization (charge 1) converts to a different class, charge 2, when the depolarization is prolonged and the channel inactivates.

A preliminary report of these results has been published (Shirokov, Levis, Shirokova, and Ríos, 1992).

METHODS

Cells

The experiments were performed on single ventricular cells enzymatically isolated from the ventricles of guinea pig hearts (strain Duncan-Hartley, 250–400 g) using 1.5 mg/ml collagenase

(type I; Worthington Biochemical Corp., Freehold, NJ) and 0.3 mg/ml protease (type XXIV; Sigma Chemical Co., St. Louis, MO) applied by Langendorf perfusion using a method similar to those of Isenberg and Klöckner (1982) and Bean and Ríos (1989). After 30–40 min of incubation in high K^+, low Na^+ solution ("KB"; Isenberg and Klöckner, 1982) cells were placed into semi-suspension culture medium (RPMI 1640) containing antibiotics (100 U/ml penicillin, 0.1 mg/ml streptomycin, and 0.2 mg/ml neomycin) and kept at room temperature before the experiments. All experiments were carried out within 24 h after separation.

Solutions

Experiments were conducted at 19–22°C. Depending on the nature of the experiments, cells were superfused with *Barium, Sodium,* or *Charge movement* solutions (see Table I). At variance with previous experiments involving cardiomyocytes, we set the pH of the internal solution at 7.8. This resulted in a significant improvement of the resolution of gating currents elicited by large depolarizing pulses. Byerly, Meech, and Moody (1984) have shown in snail neurons that

TABLE I

Ionic Composition of Internal and External Solutions

	Barium	Sodium	Charge movement	Intracellular
Na^+	—	10	—	—
Ba^{2+}	10	10	10	—
Cd^{2+}	—	—	6	—
La^{3+}	—	—	0.1	—
Mg ATP	—	—	—	5
TEA^+	166	156	154	120
HEPES	10	10	10	—
EGTA	—	—	—	10
Glucose	—	—	—	10
Creatine phosphate	—	—	—	20
$Aspartate^-$	—	—	—	80
Cl^-	186	186	186	—
pH	7.25	7.25	7.25	7.80

Values are in millimolar. Osmolality, 310 mosmol/kg. TEA^+, tetraethylammonium.

the use of an intracellular solution of higher pH efficiently blocks an H^+ outward current, which in our case would mask the gating currents at voltages more positive than +20 mV. The voltage dependence and kinetic properties of charge movement were not noticeably different for intracellular solutions with high (7.8) and normal (7.25) pH.

Current Measurement

Currents were measured in the whole-cell mode of the patch voltage clamp technique (Hamill, Marty, Neher, Sakmann, and Sigworth, 1981). Pipettes were fabricated from borosilicate glass (Corning #7052; Garner Glass, Claremont, CA) and heat polished to a tip diameter of 2–4 μm. Their typical resistance was 2–4 MΩ when filled with the internal solution. As expected, we found that pipettes typically had a twofold higher resistance when filled with TEA^+ containing solution than with the corresponding Cs^+ solution. TEA^+ was used in these experiments because an outward component of ionic current with slow activation and deactivation kinetics appeared at positive voltages in Cs^+.

Voltage clamping, pulse generation, and data acquisition were done with a commercial patch voltage clamp and associated hardware (Axopatch 1 series patch clamp with Axolab interface; Axon Instruments, Inc., Foster City, CA) under an IBM AT computer control running PCLAMP software (Axon Instruments, Inc.). Currents were normally filtered at 1 kHz (−3 dB, 4-pole Bessel filter) and sampled at 50–100 μs/point using a 12-bit A-D converter.

The whole-cell capacitance circuitry of the Axopatch 1 was modified to allow compensation of linear capacity transients from cells of up to 300 pF. This analog compensation allows the cancellation of the large majority of the linear capacity transient arising from step voltage commands by injecting an appropriate current through a capacitor directly into the headstage input. The linear current is not simply masked; instead the current is actually supplied by the capacitor, thereby minimizing the voltage excursions of the headstage output. This is of considerable importance when using most patch voltage clamps with a P/N pulse protocol. Not only does this compensation prevent possible saturation of the headstage output, but it also eliminates a potentially serious nonlinearity from the measurements. High valued resistors (several hundred megaohms and above) often suffer from small but significant voltage-dependent changes in resistance. Such nonlinearities can become quite important when P/N protocols are used to measure nonlinear charge movement, which is a small fraction of the total charging current. Tests with analog model cells and a P/−4 pulse protocol demonstrated that with our system no significant artifacts result if the output of the headstage remains less than ±1–2 V. Because of this we carefully compensated for the linear capacity transient in all measurements reported here.

After establishing the whole-cell configuration, the access resistance was typically in the range of 5–10 MΩ, although we observed series resistance (R_S) values as low as 3 MΩ and used cells with initial values of R_S as high as 15 MΩ. We often observed that the series resistance increased gradually with time. Cell input capacitance generally was in the range of 100–250 pF. These parameters were calculated from the Axopatch compensation circuitry (recalibrated after the modification mentioned above) or from control pulse transient waveforms. Series resistance was routinely compensated 70–90%; precautions were taken to avoid overcompensation and high frequency oscillations. If series resistance increased as the experiment proceeded, compensation was periodically adjusted.

Asymmetric Currents

The holding potential (h.p.) was usually in the range of −80 to −110 mV; control pulses for the conventional P/−4 procedure were applied from voltages more negative than −120 mV and maintained for 100 ms before the control pulse sequence, and individual control pulses were separated by 100 ms. The sets of pulses were applied with a frequency of not more than 0.2 Hz. These precautions were taken to avoid contamination of our controls with nonlinear charge movement (of the charge 2 type, which in skeletal muscle exhibits its steepest voltage dependence precisely in the range where control "linear" capacitive currents were obtained; Brum and Ríos, 1987). Contamination of the controls with charge 2 was an especially serious concern when conditioning depolarizations intended to cause inactivation preceded the test pulse. To avoid the problem, the determination of control currents preceded the application of the inactivating pulses in all cases.

We were not able to obtain control currents at positive voltages where all asymmetric charge movement would be saturated (Brum and Ríos, 1987). With such a procedure charge movement records were contaminated by a substantial nonspecific outward leak current. Another approach would have been to estimate the amount of charge 2 remaining in normally polarized cells by measuring charge 1 repriming when the membrane is repolarized. However, we were not able to keep cardiomyocytes depolarized for periods longer than a few seconds.

With our experimental conditions the cells became leaky and the series resistance was unstable at a holding potential of 0 mV.

The asymmetric current was obtained as the sum of the currents from the test and control pulses. All records illustrated in this paper are obtained from single test and multiple control sweeps. The data were not analyzed if the linear capacity transient changed during the control pulses so that artifacts due to residual linear current were apparent, or if records had substantial time-varying ionic current components (usually outward at positive potentials). The intramembrane charge moved by test voltage steps was measured by integrating the transient asymmetric current above a reference level computed, for test potentials ≤ -30 mV, as the average current for 5–10 ms before the test pulse; the average current for 5–10 ms at the end of the test pulse was used for test potentials > -30 mV.[1] No sloping baseline correction was made in any case.

Statistics

Measured values are given as sample average ± SEM. Theoretical functions were fitted to data using commercial, least-squares, derivativeless software (SigmaPlot; Jandel Scientific, Corte Madera, CA). Fitted values are followed by their standard error of estimate (square root of the diagonal element in the covariance matrix) in parentheses. Significance of differences of averages is established (at the $P < 0.05$ level) using the normal distribution function and conventional estimates of standard deviation of the difference; significance of average differences is established with the two-tailed t test.

Quality of Voltage Clamp Control

The significance of the experimental results described in this paper depend on the quality of transmembrane potential control. Two aspects of the voltage clamp deserve early comment:

(*1*) Spatial homogeneity of potential is a possible problem considering the rather complex geometry of ventricular cell surfaces. However, in comparison to skeletal muscle fibers, the openings of the T-tubules to the extracellular space in cardiomyocytes are clearly seen and their diameter is significantly larger (0.1–0.3 μm). Thus, morphological as well as functional evidence exists for a relatively low resistance pathway between the T-tubule lumen and extracellular space (Fawcett and McNutt, 1969; Legato and Langer, 1969). Delayed charging of the T-tubule membrane with respect to the surface membrane, due to different series resistance, would result in distinct components in the linear capacity transient measured at very negative voltages where there is presumably no asymmetric charge movement.

A representative example of currents elicited by voltage steps from −150 to −140 mV, with different levels of series resistance compensation, is shown in Fig. 1 (*A* or *B*). The two linear capacity transients illustrated represent no compensation and ~90% compensation, both filtered at 1 kHz (−3 dB, 4-pole Bessel filter). A single exponential fits well the falling phase of the uncompensated transient (not shown). There is no sign of a slow component in either of the transients.

In general, we found no evidence of slower T-tubule charging, even with our fastest response times in which the linear capacity transient was complete in ~200 μs (as observed with a 5–10-kHz filter). In recent impedance measurements conducted by R. T. Mathias (personal communication) the linear electrical properties of guinea pig ventricular myocytes were well

[1] This procedure avoided losing a small, slowly decaying component in the ON asymmetric current, which was sometimes observed for pulses below −30 mV. At higher potentials the presence of nonlinear ionic currents precluded use of the current before the pulse as reference.

described by a single parallel RC circuit up to frequencies of at least 1–2 kHz; no cable delays attributable to the T system were observed.

(*2*) The cell in Fig. 1 had a rather high value of series resistance (13 MΩ), but the records demonstrate that even in such situations adequate voltage clamp speed and time resolution can be achieved by means of series resistance compensation. Series resistance compensation both increases the speed with which the command potential is established across the cell membrane and extends the effective bandwidth of current measurement. In the presence of large ionic currents such compensation is also important in minimizing IR drops across the access resistance which could otherwise seriously degrade the adequacy of voltage control.

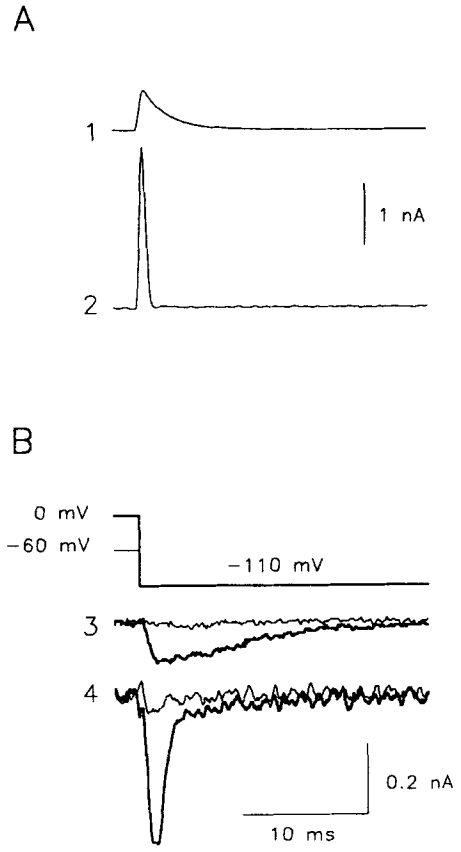

FIGURE 1. Effect of series resistance compensation on the time course of linear capacitive and OFF charge movement currents. (*A*) Capacitive transients obtained with a step from −150 to −140 mV, without (*1*) and with (*2*) series resistance compensation. The records shown are single traces. (*B*) OFF asymmetric currents from the same cell after 50-ms-long pulses to −60 mV (*thin lines*) or 0 mV (*thick lines*) without (*3*) and with (*4*) series resistance compensation. Same compensation settings as for *1* and *2;* series resistance values are 12.7 and 1.3 MΩ, respectively, without and with compensation; C_M = 154 pF; h.p. −110 mV; bandwidth 1 kHz; cell #91103C11.

The records in Fig. 1 *B* represent OFF asymmetric currents elicited from the same cell upon returning the potential to −110 mV after 50-ms test pulses to −60 and 0 mV. The upper records (labeled 3) were recorded in the absence of series resistance compensation and the lower ones (labeled 4) were measured with the same 85–90% level of compensation used for record 2 in Fig. 1 *A*. The kinetic resolution is greatly enhanced; without series resistance compensation the OFF charge movement for the −60-mV pulse is virtually invisible and the presence of two components in the OFF current for the test pulse to 0 mV is almost completely obscured. It is also clear that, by increasing the bandwidth, series resistance compensation inevitably increases the noise.

Nomenclature

The dull but time-tested term intramembrane charge movement is used here to designate the current attributable to intramembranous charged particles. It is thus synonymous with nonlinear capacitive current. Asymmetric current is an operational term, defining the method used to obtain a current that may have ionic as well as capacitive components. In the conditions of our experiments intramembrane charge movements are almost identical to asymmetric currents, except for a baseline correction of the ON, which, as described, was only carried out at high voltages. The integral of the charge movement records is here termed charge moved, or simply charge. The term gating current is usually reserved for cases where the association of the charge movement with a certain type of channel has been demonstrated.

RESULTS

This section consists of two parts: first we separate two components of intramembrane charge movement that can be ascribed to Na and Ca gating currents, and show that the latter comprises most of the mobile charge in these cells. Later we characterize two classes of charge movement, which are very similar to charges 1 and 2 of skeletal muscle.

Activation of Gating Currents

The general characteristics of nonlinear charge movement in ventricular myocytes held at −110 mV are illustrated in Fig. 2. Charge movement could be recorded with test pulses starting at −80 mV. Both the ON and OFF transients evoked by test depolarizations up to −60 mV had a fast time course, finishing within several milliseconds. In the range of −60 to −40 mV the ON transient often had a slowly decaying component with a time constant on the order of 100 ms. The significance of the slow kinetic ON component is not a topic of this study, but is consistent with a model of inactivation of the Ca channel developed in the Discussion.

In addition to a fast component, the OFF charge movement had a distinct slow component at test potentials beyond −40 mV, with a decay time constant of 11–12 ms. The resolution of the kinetics of the fast OFF component, with a decay time constant of 0.5–1.0 ms, was to some extent limited by the voltage clamp speed and the response of the 1-kHz filter.

Total charge transferred was calculated as the area under the current transient and plotted in Fig. 3. The ON values are represented as open symbols and the OFF values as filled symbols. Since it is expected that the mobile charge originates primarily from Ca and Na channels (Bean and Ríos, 1989), experimental values were fitted by the sum of two two-state canonical ensemble ("Boltzmann") distributions

$$Q = Q_{C_a} + Q_{N_a}$$

$$Q_{C_a} = \frac{Q_{\max C_a}}{1 + e^{-(V - \bar{V}_{C_a})/K_{C_a}}} \tag{1}$$

and a similar term for Q_{Na}. Q_{max} is the total amount of observable charge, $\bar{V}$ is the transition voltage, and K is the steepness factor. The best fit parameter values for nine cells and their averages are listed in Table II.

The transition voltages of the two Boltzmann components were separated by ~30 mV. The total charge carried by the low voltage component ($\overline{V}$ = −48 mV, presumably the Na channel) was approximately fourfold smaller than the charge carried by the other component ($\overline{V}$ = −18 mV, presumably the Ca channel) and more steeply dependent on voltage (K = 10 and 19 mV, respectively). All these differences were statistically significant.

Gating Current–Ionic Current Correlation

To test the hypothesis that the more negatively distributed component results from the gating of Na channels (Field et al., 1988; Bean and Ríos, 1989; Hadley and Lederer, 1989) we measured inward ionic currents and intramembrane charge movement on the same cells.

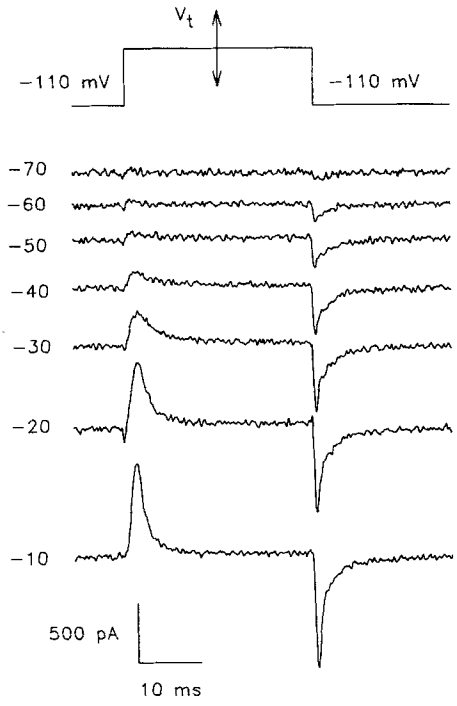

FIGURE 2. Asymmetric charge movement currents in a guinea pig ventricular myocyte. Here and in subsequent figures the double arrow marks the pulse parameter varied among records. Test voltages (V_t) are indicated near the records. Single sweeps; cell #91830C37; C_M = 230 pF.

The experiments are illustrated in Figs. 4 and 5. In *Barium* solution (Fig. 4 *A*) inward ionic currents started to activate at ~ −50 mV. The current–voltage relationship peaked at ~ −20 mV (Fig. 5, squares). In the experiment illustrated, the Ba current had almost completely run down after 20 min. At this point we changed the external solution to *Sodium*. In this situation inward current started to activate at −60 mV (Fig. 4 *B*) and the current–voltage relationship peaked at −40 to −30 mV (Fig. 5, triangles). We later measured charge movement in the same cell, switching to the appropriate solution; the charge movement currents are in Fig. 4 *C*.

The records at different voltages illustrated in Fig. 4 show that Na channels were almost fully activated at potentials more positive than −30 mV. At these potentials

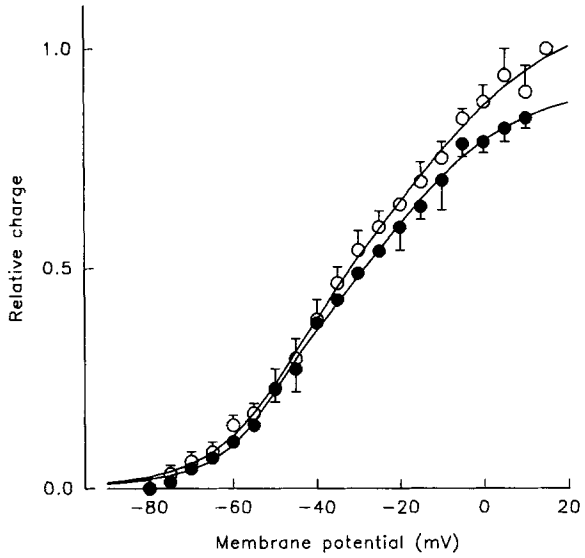

FIGURE 3. Voltage dependence of charge movement. Data from three cells. Voltage protocol illustrated in Fig. 2. *Open circles,* ON; *filled circles,* OFF. Curves generated with the equations:

$$Q_{ON} = 0.32/\{1 + \exp[(47.0 - V)/8.6]\} + 0.78/\{1 + \exp[(16.0 - V)/17.5]\}$$

and

$$Q_{OFF} = 0.18/\{1 + \exp[(51.0 - V)/5.7]\} + 0.73/\{1 + \exp[(24.5 - V)/15.5]\}$$

Voltage units are millivolts. Data were normalized individually in each cell to the ON charge at +15 mV, which was on average 10.9 (1.7) nC/μF. The increasing discrepancy between ON and OFF values is later shown to correspond to inactivation during the pulse.

TABLE II

Two-Boltzmann Fits to Q vs. V Data in Myocytes Held at −110 mV

		Q_{ON}						Q_{OFF}					
Cell No.	C_M	V_{Na}	K_{Na}	Q_{Na}	V_{Ca}	K_{Ca}	Q_{Ca}	V_{Na}	K_{Na}	Q_{Na}	V_{Ca}	K_{Ca}	Q_{Ca}
	pF	*mV*	*mV*	*nC/μF*	*mV*	*mV*	*nC/μF*	*mV*	*mV*	*nC/μF*	*mV*	*mV*	*nC/μF*
91920C01	282	−55.0	12.1	4.5	−38.8	9.3	9.9	−47.4	7.8	4.5	−25.0	15.7	7.7
91920C25	186	−44.1	7.6	2.9	−10.4	15.1	14.2	—	—	0	−16.9	14.7	15.5
91920C62	108	−58.6	7.4	1.3	−19.0	22.1	14.3	−38.8	2.3	1.4	5.6	23.8	15.7
R1920C18	117	−48.3	24.5	3.0	−20.9	13.9	16.1	−34.9	0.2	0.8	−18.8	15.6	16.6
91828C11	180	−41.6	6.8	3.2	−25.2	22.2	7.4	−45.6	8.1	2.7	−25.2	24.6	5.7
91828C18	200	−44.6	12.1	4.3	−9.4	14.9	5.3	−45.2	10.1	3.8	−17.3	13.8	4.7
91828C33	87	−40.3	5.4	2.8	−2.4	27.7	15.9	−39.8	2.6	1.5	−7.7	24.8	17.0
91830C01	297	−44.1	3.2	1.3	−25.2	18.3	6.2	−42.6	4.1	0.9	−22.0	15.8	7.6
91830C37	225	−57.5	7.4	3.8	−13.3	23.3	12.1	−57.6	7.0	3.7	−11.9	17.1	12.0
Average	187	−48.2	9.6	3.0	−17.9	18.5	11.2	−43.6	5.2	2.1	−15.4	18.4	11.4
SEM	25	2.3	2.1	0.4	3.4	1.9	1.4	2.4	1.2	0.5	3.2	1.5	1.7

The sum of two Boltzmann terms (Eq. 1) was fitted independently to ON and OFF data. The parameters of the two terms are distinguished by subindices. Subindex NA identifies the low voltage component. V, K, and Q are the transition voltage, the steepness factor, and the maximum charge, respectively. The fitting was done with six free parameters, with the exception of Q_{OFF} of #91920C25, where a $Q_{Na} = 0$ had to be imposed to achieve convergence.

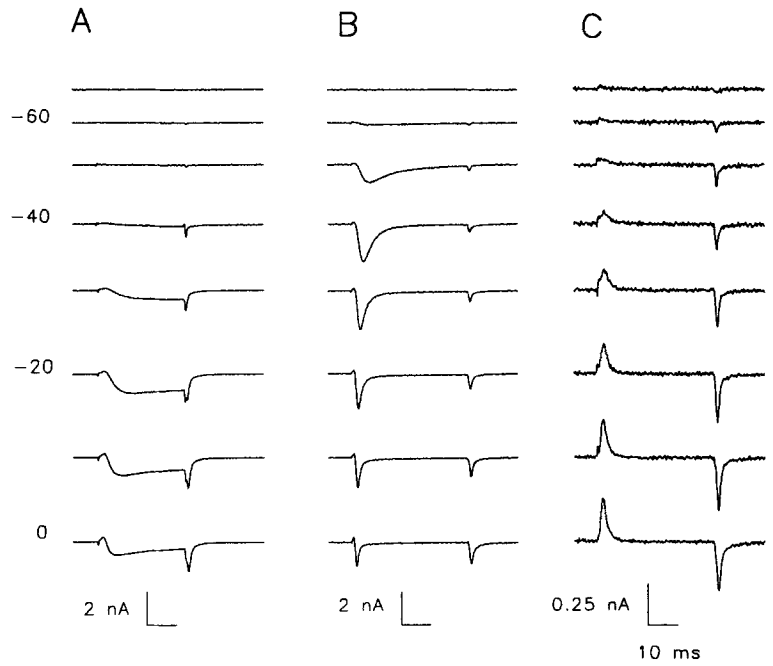

FIGURE 4. Charge movement and activation of Ba^{2+} and Na^+ currents. Currents elicited by pulses from h.p. −110 mV to the voltages indicated. (*A*) Ba^{2+} currents; records obtained after 3.5 min of cell perfusion with *Barium* solution. (*B*) Na^+ currents; recorded in *Sodium* solution after rundown of Ba^{2+} currents. (*C*) Asymmetric currents in the same cell perfused with *Charge movement* external solution. Note change of scale in *C*. Cell #91822C15; C_M = 132 pF.

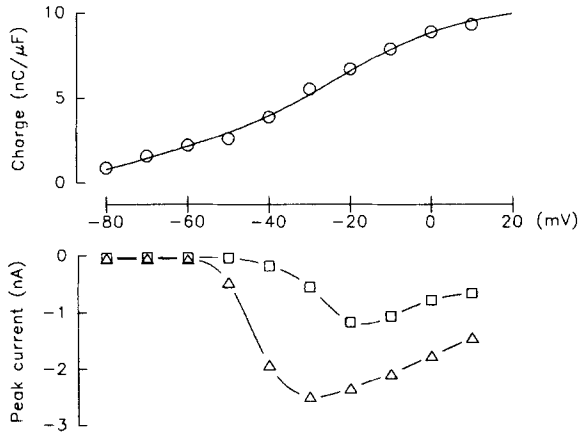

FIGURE 5. Voltage dependence of charge movement and ionic currents. *Circles*, ON charge (time integrals of ON transients in Fig. 4 *C*); *triangles*, peak amplitudes of Na^+ current; *squares*, peak Ba^{2+} current. Data for ON charge fitted by the equation:

$$Q_{ON} = 1.6\ \text{nC}/\mu\text{F}/\{1 + \exp[(73.5 - V)/9]\} + 8.9\ \text{nC}/\mu\text{F}/\{1 + \exp[(24 - V)/16.2]\}$$

Voltage units are millivolts. Other data are connected by spline curves. All data were obtained from records in Fig. 4.

the activation of the first Boltzmann component of charge movement was essentially complete, whereas that of the second component had just started. These observations indicate that the component activating at more negative potentials is the charge movement of Na channels. The second component is presumably the charge movement of high voltage-activated (L-type) Ca channels.

Separation of Sodium and Calcium Gating Currents Based on Availability Measurements

The experiments described above suggested that Na channel gating current accounted for ~25% of the total nonlinear charge movement. A more precise separation of the two components based on differences in the voltage dependence of their activation was difficult because the differences in the transition voltages were small relative to the steepness of the distributions.

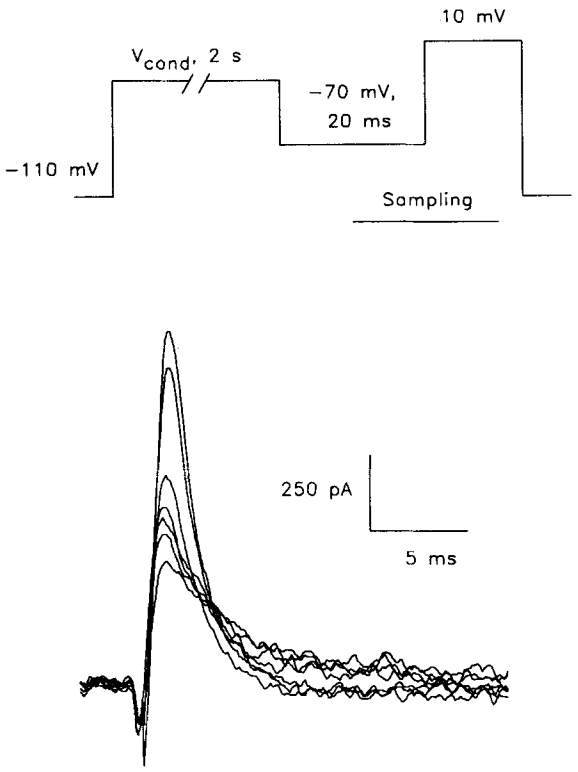

FIGURE 6. Effect of 2-s conditioning depolarizations on the ON charge movement. Voltage protocol is shown schematically. Asymmetric current traces at V_{cond} (from the top): −110, −90, −80, −70, −60, −50, −40 mV. Cell #91830C41; C_M = 276 pF.

Other estimates have used the different dependence of the availability of gating charge on the holding potential. In cardiomyocytes the availability of charge movement decreases in two phases as h.p. increases (Bean and Ríos, 1989; Hadley and Lederer, 1989), presumably corresponding to Na and Ca channel inactivation. The same method was used here, with the result that a major portion of the charge inactivated (became unavailable to move, but compare below) with the voltage dependence of Ca channel inactivation.

Fig. 6 shows the pulse protocol used and a family of currents. Different potentials (labeled V_{cond}) were imposed for 2 s; the voltage was then stepped to −70 mV for 20 ms and a test pulse was applied to +10 mV, a potential sufficiently high to move essentially all the charge available. The charge moved by this pulse during the ON is termed Q_R.

Q_R (V_{cond}) is termed the availability function, and is shown in Fig. 7 (open circles) together with the activation curve determined from an h.p. of −110 mV on the same cells (filled circles). Results from individual cells were averaged after normalization to

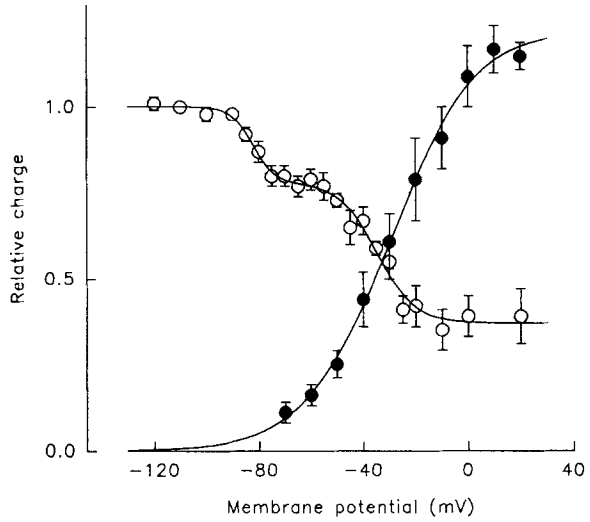

FIGURE 7. Charge movement activation and availability curves. *Open circles,* availability, charge that moves during the ON of the test pulse in the pulse protocol of Figure 6, plotted as a function of V_{cond}. Data fitted by the equation:

$$Q_R = 0.36 + 0.23/\{1 + \exp[(V + 82.3)/4.5]\} + 0.41/\{1 + \exp[(V + 34.5)/7.1]\}$$

Filled circles, activation, ON charge moved by a pulse to the voltage in the abscissa, from a h.p. of −110 mV. Data fitted by the equation:

$$Q_{ON} = 0.34/\{1 + \exp[(45.7 - V)/15.4]\} + 0.89/\{1 + \exp[(24.0 - V)/14.6]\}.$$

Voltage units are millivolts. Both sets of data were obtained from the same seven cells. Values from individual cells were first normalized to the charge available at V_{cond} = −110 mV (no conditioning) and then averaged. The average charge available at −110 mV was 12.3(1.3) nC/μF.

the value of charge available at h.p. −110 mV. The amount of charge moved from −70 to +10 mV was about constant for V_{cond} in the range of −120 to −90 mV. At V_{cond} = −70 mV the availability decreased by ~20%. Thereafter, charge availability remained constant up to about −50 mV; then it again decreased, reaching a steady level of one-third its initial value by −25 mV. The time constant of exponential decay for the ON transients at +10 mV increased from 1.5 (0.2) to 2.8 (0.3) ms between V_{cond} = −120 and −50 mV.

The Q (V) data (filled circles) were fitted by the sum of two Boltzmann terms. The availability data (open circles) were fitted by the sum of two Boltzmann terms and a constant. Table III presents individual fitted values and average parameters. The continuous lines in Fig. 7 were generated with the best fit to the average points shown (they are similar but not identical to the curves generated with the average parameters in the table).

The average amplitude of the Na channel component of the Q (V) relationship (Q_{Na} in Table 3) was 3.4 nC/μF. The low voltage component of the availability (Q_{RNa}) was 2.5 nC/μF (not a statistically significant difference). A difference of this magnitude was expected, however. Indeed, the probing pulse in the availability determinations went from −70 to +10 mV. As shown in Fig. 3, this voltage swing

TABLE III

Fits to Availability and Activation of Charge Movement and Two-Boltzmann Cannonical Fits to the ON Charge Movement Q vs. V Curves

	Q_R							Q_{ON}					
Cell No.	Q_{RS}	$\bar{V}_{RNa}$	K_{RNa}	Q_{RNa}	$\bar{V}_{RCa}$	K_{RCa}	Q_{RCa}	$\bar{V}_{Na}$	K_{Na}	Q_{Na}	$\bar{V}_{Ca}$	K_{Ca}	Q_{Ca}
	nC/μF	*mV*	*mV*	*nC/μF*	*mV*	*mV*	*nC/μF*	*mV*	*mV*	*nC/μF*	*mV*	*mV*	*nC/μF*
91830C41	3.0	−77.3	3.8	3.0	−30.8	7.8	6.9	−55.1	9.4	3.5	−20.0	10.3	9.5
91920C01	1.9	−84.8	6.6	3.4	−27.9	6.2	4.2	−55.0	12.1	4.5	−35.8	9.2	9.9
91920C25	2.8	−76.0	5.9	3.7	−25.8	7.7	6.2	−44.0	7.6	2.9	−10.4	15.0	14.1
91920C62	4.6	−79.3	3.2	1.8	−28.0	13.6	5.1	−54.5	3.0	2.1	−19.7	12.8	12.0
R1920C18	6.2	−80.0	5.2	2.3	−19.3	12.2	7.5	−48.3	24.5	3.0	−20.9	13.9	16.0
R1920C62	1.8	−88.6	4.6	2.4	−34.5	7.1	8.4	−58.6	7.4	6.3	−7.4	5.8	7.7
N1920C01	4.1	−97.4	6.5	1.0	−37.4	9.6	5.5	−51.0	4.6	1.3	−19.0	22.8	14.3
Average	3.5	−83.3	5.1	2.5	−29.1	9.1	6.3	−52.3	9.8	3.4	−19.1	12.7	11.9
SEM	0.6	2.9	0.5	0.4	2.2	1.0	0.6	1.9	2.7	0.6	3.4	1.9	1.1

ON charge moved by a pulse from −70 to 20 mV (Q_R) was fitted as a function of 2 s conditioning voltage (V) by:

$$Q_R = Q_{RS} + Q_{RNa}/\{1 + \exp(V - \bar{V}_{RNa})\} + Q_{RCa}/\{1 + \exp[(V - \bar{V}_{RCa})/K_{RCa}]\}$$

ON charge moved by a pulse from −110 to V in cells held at −110 mV (Q_{ON}) was fitted by the sum of two Boltzmann terms (Eq. 1). The column headings under Q_{ON} are defined in Table II.

leaves out > 1 nC/μF of charge, which moves below −70 mV and presumably arises from Na channels. Another consequence of this restricted range of the pulse probing availability is the fact that the maximum availability in Fig. 8 is some 2 nC/μF smaller than the maximum of the activation curve. Adding 1 nC/μF to Q_{RNa}, a number equal to the low voltage component of the activation curve (Q_{Na}) is obtained. This number, 3.5 nC/μF, is our best estimate of the magnitude of Na gating charge.

A Slow Component of Charge Movement

We have already noted that for cells held at −110 mV the OFF transient had a substantial slow (exponentially decaying) component. It will be shown that essentially all of the mobile charge of a cell can be made to move in this manner, given the appropriate pulse protocol. The remainder of the Results section consists of an

examination of this component. It will be argued in the Discussion that most of it originates in Ca channels.

Fig. 8 *A* shows, in a cell held at −110 mV, that the OFF transient after 50-ms test pulses had an obvious slow component for all test potentials greater than −60 mV. The OFF gating current at −110 mV was fitted as the sum of two exponentials. The time constant of the fast term was 0.7 (0.2) ms (n = 7) and was probably limited by

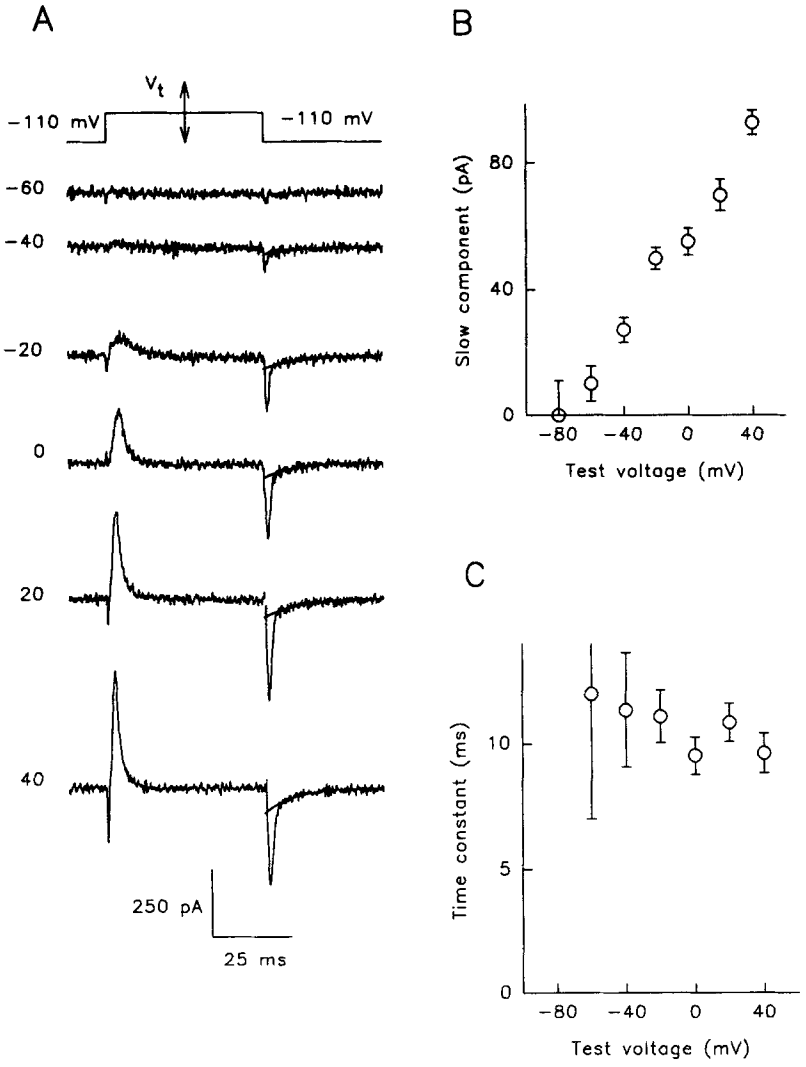

FIGURE 8. Activation and kinetics of the slow OFF charge movement. (*A*) Asymmetric currents from a cell held at −110 mV pulsed to the indicated voltages. The smooth lines are single-exponential fits to the slow OFF component. (*B*) Amplitudes of the fitted slow component extrapolated to zero as a function of test voltage V_t. (*C*) Best fit time constants of the slow component. In *B* and *C* bars correspond to standard error of the estimate. Cell #91102C02; C_M = 165 pF.

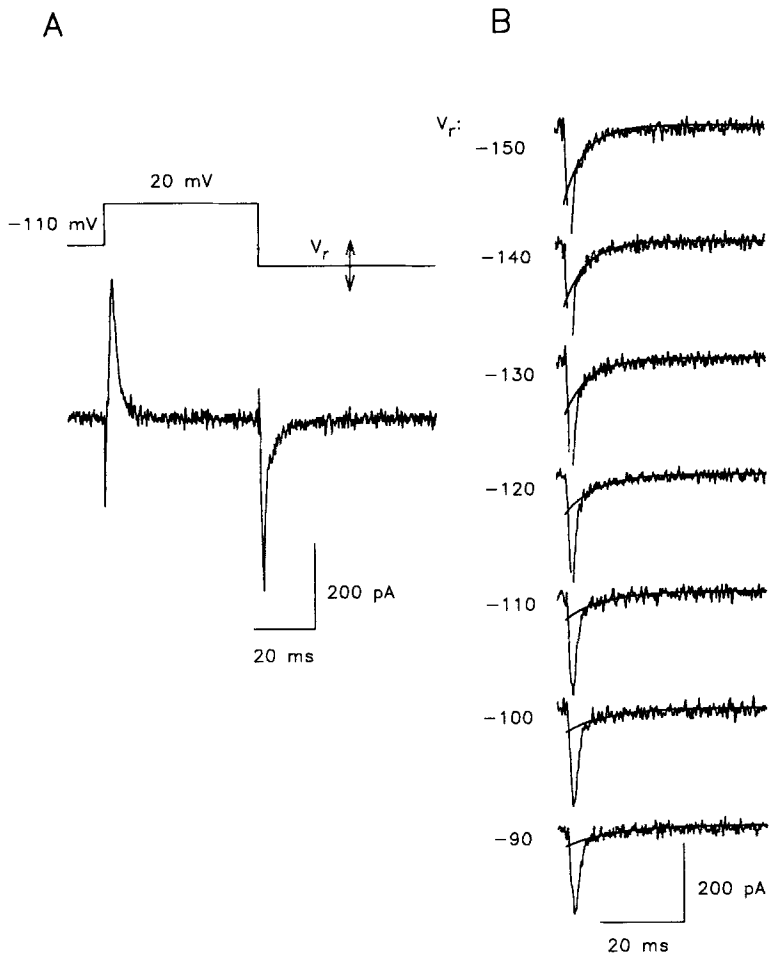

FIGURE 9. The slow component at different repolarization voltages. (*A*) Asymmetric current obtained with the pulse protocol shown; 50-ms test pulse from −110 mV to +20 mV and repolarization to −150 mV. (*B*) OFF currents obtained at different repolarization voltages. Superimposed lines are single-exponential fits to slow component. Parameters of fit are given below in the sequence: OFF voltage, amplitude, time constant. −150 mV, −215(8.6) pA, 5.0(0.17) ms. −140 mV, −169(11.3) pA, 5.5(0.3) ms. −130 mV, −114(10.3) pA, 5.9(0.35) ms. −120 mV, −105(6.2) pA, 7.3(0.41) ms. −110 mV, −74.4(8.0) pA, 8.9(0.94) ms. −100 mV, −64.5(8.4) pA, 9.6(1.28) ms. −90 mV, −56.5(5.5) pA, 11.9(1.45) ms. Cell #91102C02; C_M = 165 pF.

the clamp speed and filter bandwidth; this time constant was essentially independent of the test potential. The amplitude of the slow component increased steadily with increasing test potential as illustrated in Fig. 8 *B*.[2] In spite of the large variation in

[2] Note that the amplitude of this component is proportional to the charge carried by the slow component since under these conditions its time constant was invariant. Also note that the activation of this slow component did not reach saturation even at the highest test voltages. It is shown later (Fig. 15) that such saturation occurs at longer pulse durations.

amplitude, the slow time constant was also independent of test potential (Fig. 8 *C*) having an average value of 11.8 (0.6) ms ($n = 7$). In fact, we found that the time constant of the slow component was independent of the test potential for any fixed repolarization potential in the range of −150 to −60 mV. As will be seen below, however, this time constant does depend on the value of the repolarization (OFF) potential.

Fig. 9 shows an example of OFF transients measured for different repolarization potentials after a fixed 50-ms depolarization to +20 mV. The lines superimposed on the current traces in Fig. 9 *B* are the best fits to the slow component; each has a different time constant, with a maximum of 12.4 (2.0) ms ($n = 7$) for OFF potentials in the range of −90 to −110 mV to 4.6 (0.8) ms ($n = 7$) at −150 mV.

Time constants of the slow component, collected from eight cells, are plotted in Fig. 10 as a function of the OFF potential. The open triangles are for test

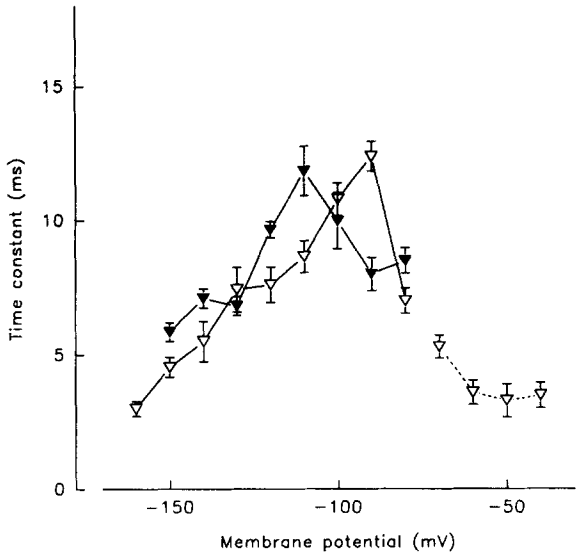

FIGURE 10. Voltage dependence of the slow component time constant. *Open triangles,* test pulse to +20 mV. *Filled triangles,* test pulse to −30 mV. Values were obtained by two-exponential fits to the OFF current, except at voltages from −70 to −40 mV, where they were obtained by single exponential fits. Averages from 14 cells. Vertical bars represent standard errors of the mean.

depolarizations to +20 mV and the closed triangles are for test depolarizations to −30 mV. Data obtained in the region from −70 to −40 mV are separated from the main group because they were calculated by a single exponential fit rather than the double exponential fit that was possible for more negative repolarization potentials. In spite of some differences at the two test potentials used, the dependence of the slow component time constant on repolarization potential had a bell shape with a maximum of ~12 ms near −100 mV.

From a simple (symmetrical) one-barrier scheme of charge transfer it is expected that the maximum of the charge movement time constant occurs at the midpoint voltage of the activation relationship, where the probabilities of forward and backward transitions are equal. Therefore the slow component of OFF asymmetric current is likely to be a charge movement centered at very negative potentials. As will be amply demonstrated later, the properties of this charge movement are almost

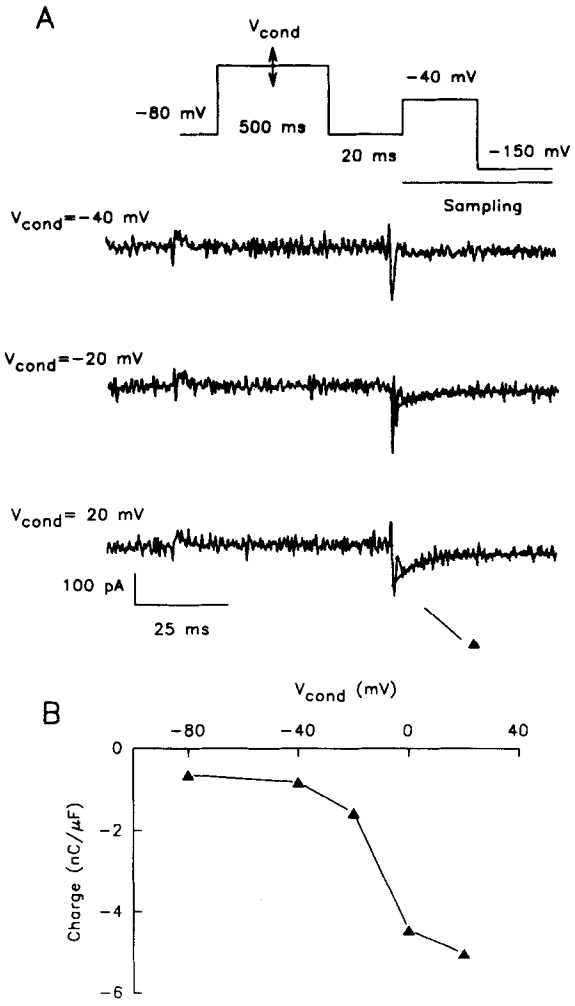

FIGURE 11. Slow charge movement as a function of conditioning pulse voltage. (*A*) Current traces obtained by the pulse protocol shown at top with different conditioning voltages listed near the traces. Exponential fits to the slow component have the same time constant (5.0 ms) at both −20 and +20 mV. (*B*) Total charge moved by the transition from −40 to −150 mV, (OFF integrals of records in *A*) for different conditioning voltages. Cell #91103C30; C_M = 111 pF.

identical to those of charge 2 of skeletal muscle (Adrian and Almers, 1976; Brum and Ríos, 1987). Consequently, the ensuing experiments are based on the work carried out previously in skeletal muscle to explore the properties of this charge.

Conditioning Parameters Determine the Magnitude of the Slow Charge

The magnitude of the slow component of charge movement increased after large or prolonged depolarizations. The onset of the slow charge during depolarizing pulses was studied with pulse protocols such as shown in the upper panels of Figs. 11–13. The total charge transferred by the OFF voltage step from −40 to −150 mV was used as quantifier of the magnitude of the slow charge.[3] The variables were the condition-

[3] This involves an error due to the presence of a fast component (e.g., top record in Fig. 11). The charge carried in this fast component was, however, < 1 nC/μF in all cases.

ing pulse amplitude (Fig. 11 *A*), its duration (Fig. 12 *A*), and the delay between the conditioning and test pulses (Fig. 13 *A*).

Fig. 11 *B* plots the relationship between the amount of OFF charge and the conditioning voltage. The ordinate (charge) is represented negative, as it is carried by an inward current. Except for this negative sign, the Q (V_{cond}) dependence was similar to the Q (V) relationship measured without conditioning pulses in a conventional activation experiment (Fig. 3).

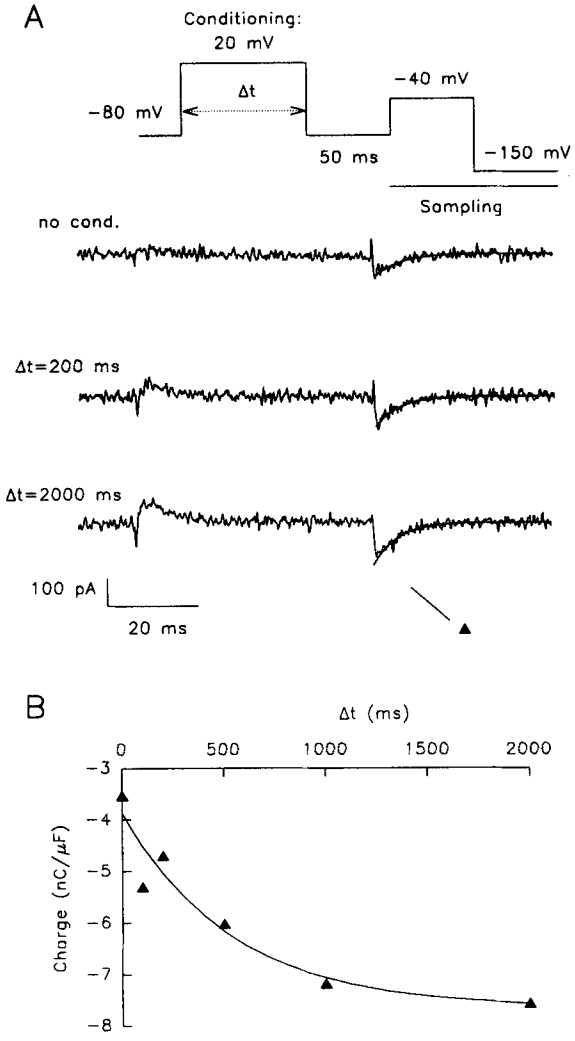

FIGURE 12. Slow charge movement as a function of conditioning pulse duration. (*A*) Asymmetric currents obtained with the pulse protocol shown at top, with variable duration (Δt) of conditioning and a 50-ms test pulse. Exponential fits to the slow component have a time constant of 5 ms (top two records) or 5.4 ms (bottom record). Essentially the same OFF time constant (5 ms) was adequate for all records in the experiments illustrated in Figs. 11–13. (*B*) Total OFF charge as a function of conditioning pulse duration. The exponential fit (*solid line*) has a time constant of 540 ms. The nonzero intercept suggest the existence of a component of very fast onset in charge 2. Cell #91103C64; C_M = 192 pF.

Increasing the conditioning pulse duration increased the amount of slow charge. One determination of the time course of this process is illustrated in Fig. 12 for a conditioning pulse to +20 mV. The time constant of a single exponential fit to the data shown is 540 ms (480 ± 137 ms, n = 3). The parameter is presumably voltage dependent, but was not determined at other conditioning voltages.

The slow charge elicited by long depolarizations decreased in magnitude as a gap of increasing duration (Δt) was included between the conditioning and the test pulses. Fig. 13 illustrates the effect for a conditioning pulse of 500 ms to 0 mV. The plot of slow OFF charge vs. Δt was well fitted by an exponential decay with time constant 220 ms (158 ± 24 ms, n = 4).

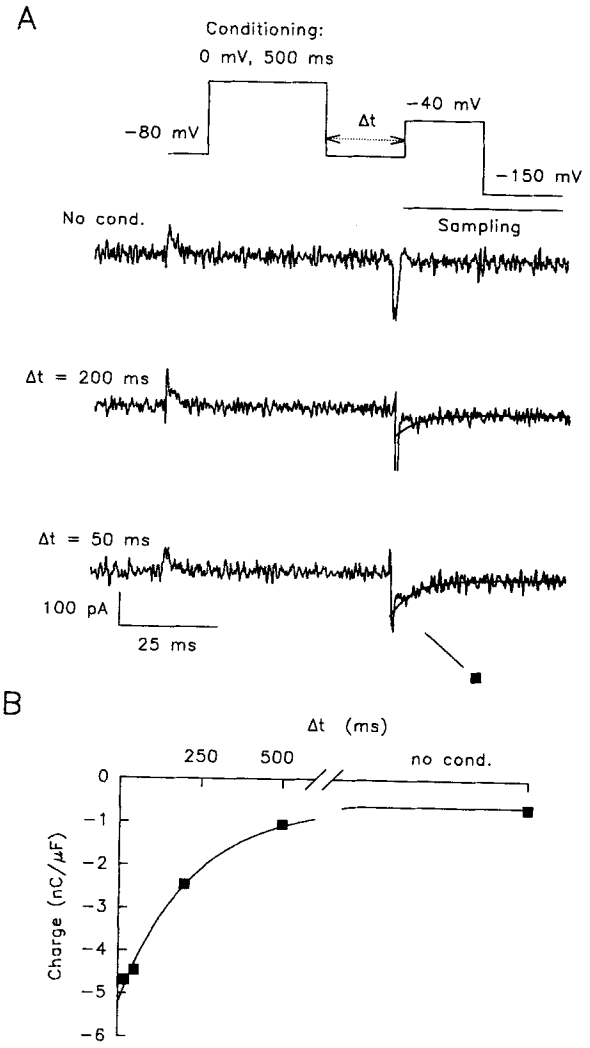

FIGURE 13. Slow charge movement after different delays between conditioning and test pulse. (*A*) Asymmetric currents obtained with the pulse protocol shown at top, where the variable is the interval (Δt) between conditioning and a 50-ms test pulse. The record and point labeled "No cond." corresponds to an interval of 10 s between the test and the previous pulse. (*B*) Total charge moved by the OFF transition from −40 to −150 mV as a function of Δt. The decay followed a single exponential (*solid line*) with a time constant of 220 ms. Cell #91103C26; C_M = 120 pF.

Change in the Voltage Dependence of Intramembrane Charge after Prolonged Depolarization

The changes in voltage dependence of charge movement that accompany prolonged depolarization are demonstrated in Table IV, which summarizes a study at three voltages in many cells, and in Figs. 14 and 15, illustrating studies at different

voltages. When a cell is at a h.p. of −110 mV, a depolarizing pulse from −110 to +20 mV moves almost all the intramembrane charge available, whereas a pulse from −110 to −60 mV moves very little charge. This fact is illustrated for several cells by columns 1 and 2 of Table IV. The voltage step back to −110 mV evoked nearly the same amount of OFF charge movement (column 5) as was obtained at the ON transition (column 1). On the other hand, after the depolarizing test pulse the charge moved when the membrane was repolarized from +20 to −60 mV was at least 40% less than the ON charge moving between −60 and +20 mV (columns 4 and 3). The "missing" charge moved at more negative potentials, in the range −60 to −110 mV (columns 6 and 2).

The voltage distribution of charge movement before and after a 50-ms depolarization is illustrated in Fig. 14. First the $Q(V)$ curve was measured under normal

TABLE IV

Differences in the Voltage Distribution of ON and OFF Charge Movements Evoked by a 50-ms-long Pulse

Cell No.	1 −110 mV ↓ −60 mV	2 −110 mV ↓ 20 mV	3 −60 mV ↓ 20 mV	4 20 mV ↓ −60 mV	5 20 mV ↓ −110 mV	6 −60 mV ↓ −110 mV
91102C03	0.32	10.66	10.34	7.56	10.01	2.45
91102C17	0.00	4.89	4.89	2.33	4.66	2.33
91102C21	0.48	6.30	5.82	3.22	6.18	2.96
91102C46	0.74	4.10	3.36	1.91	4.25	2.34
91103C17	0.21	10.10	9.89	5.75	9.57	3.82
91103C49	0.47	10.44	8.97	4.45	9.24	4.79
Average	0.37	7.58	7.21	4.27	7.32	3.12
SEM	0.1	1.16	1.19	0.88	1.06	0.41

Cells were held at −110 mV and pulsed to either −60 or 20 mV. The ON charge moved in the pulse to −60 is listed in column 1, and that in the pulse to 20 mV in column 2. The return from the 50-ms-long depolarization to 20 mV was done to either −60 or −110 mV. The OFF charge in the return to −60 mV is listed in column 4, and that in the return to −110 mV in column 5. Column 3 is the difference of column 2 − column 1. Column 6 is column 5 − column 4.

conditions, with test pulses starting from an h.p. of −110 mV (Fig. 14 *A*, left records; Fig. 14 *B*, circles). The effects of depolarization were then determined with the pulse protocols shown in the middle and right panels of Fig. 14 *A*. After a 50-ms depolarization to a fixed +20 mV potential (Fig. 14 *A*, middle) the charge moved at the OFF was measured at various OFF potentials and represented as triangles in Fig. 14 *B*. Charges are plotted negative, as the OFF transitions elicit inward current.

A similar study was carried out with a −30-mV depolarization (Fig. 14 *A*, right); the voltage dependence of the OFF charge after this depolarization was represented as squares in Fig. 14 *B*. The charge moved by pulses to voltages greater than −30 mV was plotted positive, corresponding to the fact that the pulse elicited outward current. Conversely, when the final potential was more negative than −30 mV the current elicited was inward and charge was plotted negative.

The result is that the pulse to +20 caused a large shift in voltage dependence (triangles). After the depolarization to −30 mV (squares) the voltage dependence was not shifted as far toward negative potentials, but its steepness decreased drastically.

The continuous lines in the plots of Fig. 14 *B* demonstrate that the apparently complicated effect can be understood as a redistribution of charge between two forms (or modes) of charge movement. Thus, the circles are described by a single Boltzmann curve with $\overline{V} = -21$ mV and $Q_{max} = 8.3$ nC/μF, a simple distribution with a fairly high transition voltage, which by analogy with skeletal muscle may be termed charge 1. The other two sets of data require two Boltzmann terms (and a constant). Both could be fitted as the sum of one term with $\overline{V}_1 = -21$ mV (charge 1) and another centered at a much more negative voltage (charge 2). The Q_{max} of charge 1 (Q_{max1}) decreased to 4.5 nC/μF after the depolarization to −30 mV, and the Q_{max} of the other term (Q_{max2}) was 3 nC/μF. After the depolarization to +20 mV Q_{max1} became 2.3 nC/μF and Q_{max2} was 5.5 nC/μF.

In spite of the large changes in the individual components, total charge was conserved, and in all three cases the sum of Q_{max1} and Q_{max2} was close to 8 nC/μF, consistent with the interpretation that the same voltage-dependent molecules were redistributed to a variable extent between two forms, one of which generates charge 1, centered at −21 mV, and the other of which generates charge 2, centered at or near −100 mV.

The above interpretation led to the hope that, given a sufficiently large and prolonged depolarization, it would be possible to convert all the available charge to the charge 2 type (as is the case for skeletal muscle; Brum and Ríos, 1987). This prediction was tested in five experiments; three experiments with identical protocols are represented in Fig. 15. First $Q(V)$ was measured by a conventional pulse protocol from a h.p. of −110 mV (filled circles). The potential was then stepped to 0 mV for 5 s, which was close to the maximum duration of depolarization tolerated by these cells, and the voltage distribution was explored again in steps from 0 mV. After each step from the 0 mV potential the cell was held at −110 mV for 10 s to insure that the distribution of charge reverted to that of a well-polarized cell (charge 1) and conventional control pulses were taken. Note that in this situation test pulses to potentials negative to the holding potential elicited no asymmetric currents. The charge distribution in depolarized cells is shown as open circles in Fig. 15. The data, in both the polarized and depolarized condition, are averages over the same three cells after normalization of individual values to the charge moved in a pulse from 0 to −150 mV.

Both sets of data could be fitted by a single Boltzmann. The transition voltage was −31 (2.6) mV in the normally polarized cells and −99 (2.5) mV after depolarization. In agreement with the observations in Fig. 15, neither the total charge (10.7 [0.3] and 10.6 [0.4] nC/μF) nor the steepness factor (16.9 [2.2] and 15.8 [1.9] mV) changed. It is important to note that the transition voltage of the distribution of charge in depolarized fibers is in good agreement with both the transition voltage of charge 2 as defined by the fits of Fig. 14 and with the voltage at which the time constant of the slow component of OFF charge movement reaches its maximum (Fig. 10).

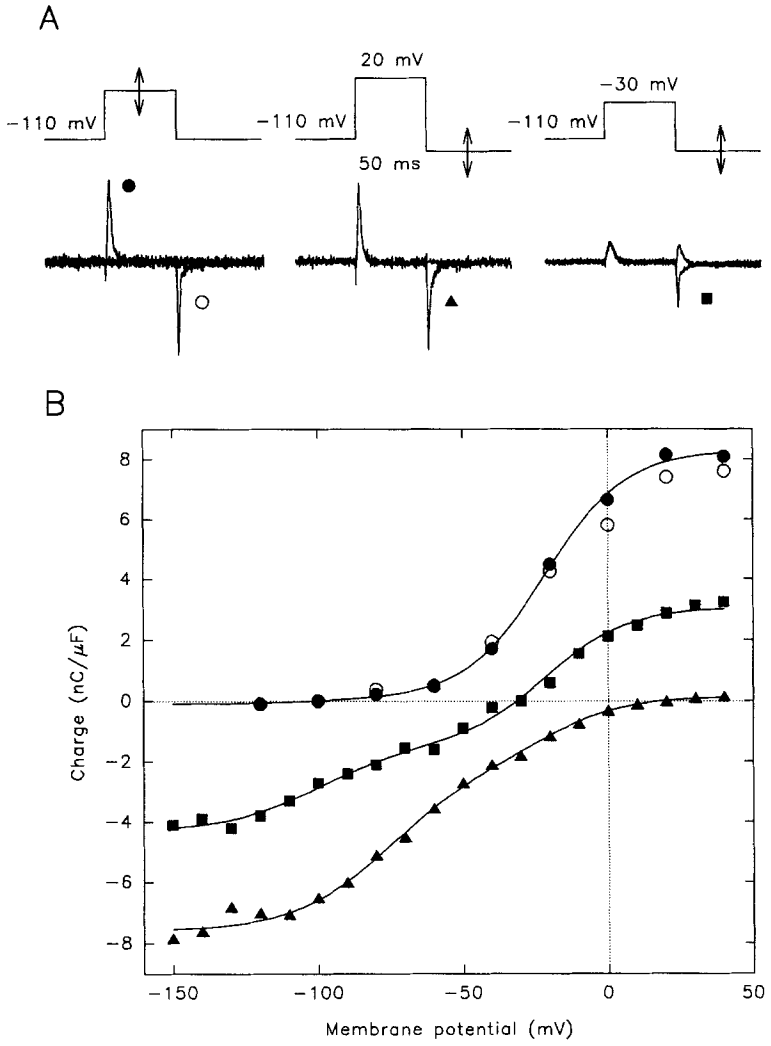

FIGURE 14. Effect of depolarization on the voltage dependence of total charge. (*A*) Pulse protocols and asymmetric current traces. In all cases the arrows indicate the variable voltage, which is represented on the abscissa in the plots of *B*. *Left*, conventional pulse protocol. Asymmetric currents elicited by tests to −80 and +20 mV are shown superimposed. *Middle*, repolarizations to different voltages follow the pulse to +20 mV. Asymmetric currents with repolarizations to −150 and +20 mV are shown superimposed. *Right*, repolarizations to different voltages follow a pulse to −30 mV. Currents with repolarizations to −150 and +20 mV are shown superimposed. (*B*) Charge moved during the transients illustrated in *A* as a function of the voltages indicated by arrows in *A*. *Filled circles*, ON charge moved by conventional voltage steps (protocol, *A*, *left*). These data, as well as other data in *B*, were fitted as the sum of two Boltzmann terms plus a constant:

$$Q(V) = Q_p + Q_{max1}/\{1 + \exp[(\bar{V}_1 - V)/K_1]\} + Q_{max2}/\{1 + \exp[(\bar{V}_2 - V)/K_2]\}$$

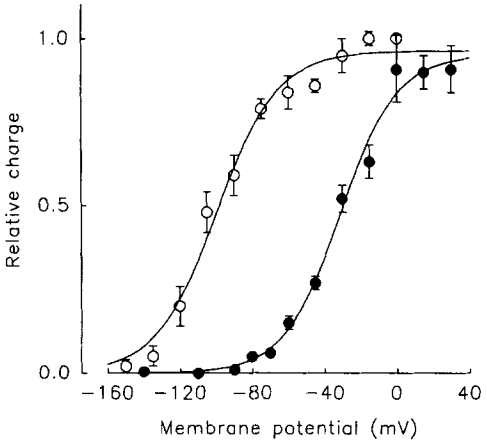

FIGURE 15. Voltage distribution of mobile charge in normally polarized and depolarized myocytes. *Filled circles,* charge measured from a h.p. of −110 mV. *Open circles,* charge measured from a h.p. of 0 mV (see details in the text). Data from three cells were averaged after normalizing in each individual cell to the charge moved by a pulse from 0 to −150 mV in the depolarized condition. The average value of the charge used for normalization was 11.2(1.1) nC/μF. Solid lines correspond to single Boltzmann fits to the averages. The parameters are given below, identifying with subindex 1 those of the normally polarized situation: Q_{max1}, 0.95(0.04); $\overline{V}_1$, −31.1(2.6) mV; K_1, 15.8(1.9) mV; Q_{max2}, 0.96(0.03); $\overline{V}_2$, −99.4(2.5) mV; K_2, 16.9(2.2) mV.

Effects of D600 on the Voltage Distribution of Charge Movement

Bean and Ríos (1989) showed in rat ventricular myocytes that the Ca antagonist phenylalkylamine D600 at 10 μM, together with a conditioning depolarization, substantially reduces the Ca channel charge movement. In frog skeletal muscle D600 is known to eliminate charge 1 (Hui, Milton, and Eisenberg, 1984) and favor the appearance of charge 2 (Feldmeyer, Melzer, and Pohl, 1990) and the conversion of charge 1 into charge 2 (Pizarro, Fitts, Rodriguez, Uribe, and Ríos, 1988; Caputo and Bolaños, 1989). We applied 100 μM D600 to the bathing solution and observed an enhancement in the effect of conditioning depolarizations on the appearance of slow charge movement.

Fig. 16 shows an example of this effect: the test pulse (V_t in the schematic protocol) went to a voltage of +20 mV (top records) or −40 mV (bottom). In a reference situation, without conditioning or drug, the test pulse at +20 mV elicited a large ON transient (top center record) followed by a large and fast OFF transient. The ON at −40 mV was small (bottom center), and the OFF from that pulse was small and very fast. A 500-ms conditioning pulse to 0 mV caused the ON at +20 to become smaller in amplitude, whereas both ON and OFF in the pulse to −40 became slower due to

FIGURE 14 (*continued*) Best fit parameters: Q_p = −0.1 nC/μF; Q_{max1} = 8.3 nC/μF, $\overline{V}_1$ = −21.3 mV, K_1 = 13.8 mV; Q_{max2} = 0.2 nC/μF, $\overline{V}_2$ = −90.8 mV, K_2 = 13.8 mV. *Open symbols,* OFF charge (protocol *A, left;* not fitted). *Filled triangles,* OFF charge moved after a 50-ms pulse to +20 mV (protocol A, *middle,* charges are plotted negative as they were all transferred by inward currents). Parameters of two-Boltzmann fit: Q_p = −7.6 nC/μF; Q_{max1} = 2.3 nC/μF, $\overline{V}_1$ = −21.0 mV, K_1 = 14.0 mV; Q_{max2} = 5.5 nC/μF, $\overline{V}_2$ = −75.5 mV, K_2 = 16.6 mV. *Filled squares,* OFF charge moved after a 50-ms pulse to −30 mV (protocol A, *right,* charges are plotted negative for voltages more negative and positive for voltages positive to −30 mV, as justified in text). Parameters of two-Boltzmann fit: Q_p = −4.3 nC/μF; Q_{max1} = 4.5 nC/μF; $\overline{V}_1$ = −21.0 mV, K_1 = 14.0 mV; Q_{max2} = 3.0 nC/μF, $\overline{V}_2$ = −99.5 mV, K_2 = 16.6 mV. Cell #90D16C41; C_M = 231 pF.

the appearance of slow charge movement. Both effects were enhanced in the presence of D600 (right panel), where the presence of a slow OFF component became obvious at both potentials. The OFF charge moved by the pulse from −40 to −150 mV was 2.1 nC/μF in reference, 4.3 nC/μF after conditioning, and 6.9 nC/μF after conditioning in the presence of D600. In three similar experiments the increase due to the drug was 77 (23)%. These effects of enhancement of the slow component are thus similar to the enhancement of charge 2 induced by D600 in skeletal muscle, and they strengthen the evidence that the slow component of current under study is charge 2. Given the fact that cardiac Na channels are sensitive to phenylalkylamines at the high concentration used here (Bayer, Kalusche, Kaufmann, and Mannhold,

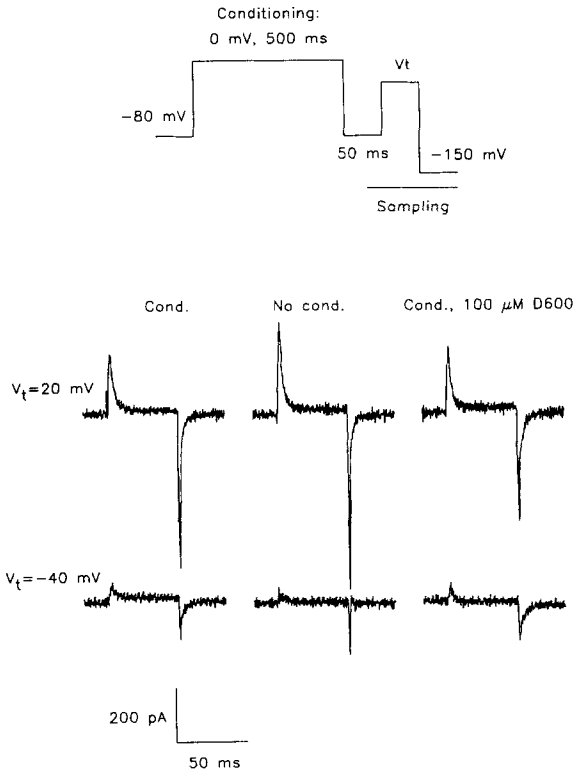

FIGURE 16. D600 increases slow charge movement. *Upper trace,* pulse protocol. The test pulse voltage was either +20 mV (asymmetric currents in first row of records) or −40 mV (bottom records). The values of OFF charge for different cases, illustrating the enhancement of slow charge by D600, are given in the text. Cell #91103C46; C_M = 153 pF.

1975), it is not possible to attribute the origin of the increased charge 2 to Ca channels alone.

DISCUSSION

Charge Movement of Guinea Pig Ventricular Myocytes Is Mostly L-Type Calcium Channel Gating Current

Measurements of charge movement from adult guinea pig ventricular myocytes aimed at determining the contribution of Na channel gating current to total charge movement led us to the conclusion that it accounts for only ~3.5 nC/μF from a total

of 14–14.5 nC/μF. This value is close to that reported by Bean and Ríos (1989)—4.2 nC/μF from a total of 11 nC/μF—but only about half of the estimate of Hadley and Lederer (1989)—7.2 nC/μF from 10.9 nC/μF in rat and 6.7 nC/μF from 11.7 nC/μF in guinea pig ventricle. The total intramembrane charge reported for ventricular myocytes from neonatal rat is ~4 nC/μF, of which Na channel gating current accounts for <1 nC/μF (Field et al., 1988).

Hadley and Lederer (1989) defined Na channel gating current as the portion of the total charge that does not move from a holding potential of −50 mV. The present results imply that this definition overestimates Na channel gating current because a substantial amount of the Ca channel charge movement moves negative to −50 mV (Figs. 3 and 4 *C*). Moreover, as evidenced by the present results, a holding potential of −50 mV will cause some redistribution of Ca channel gating current from more positively distributed charge 1 to more negatively distributed charge 2, leading to a further reduction in the measured Ca gating current.

As in previous work (Bean and Ríos, 1989; Hadley and Lederer, 1989) the availability of charge movement as a function of conditioning potential could be described by two Boltzmann components plus a constant (Fig. 7). The result of our present estimation, 3.5 nC/μF for the Na gating component, out of 14 nC/μF total charge, is substantially smaller than the estimate of Hadley and Lederer (1989) using a similar method in the same tissue and species. The reason for the difference must be found in the different pulse protocols chosen. The most crucial parameters of the double pulse protocol are duration and the voltage of the gap before the test pulse. We selected a "gap voltage" (−70 mV) sufficiently negative to include most of the Na channel component and sufficiently positive to avoid substantial recovery from Na channel inactivation. The duration (20 ms) was brief to avoid recovery, but sufficient to allow the establishment of a steady baseline current.

The gap parameters used by Hadley and Lederer (1989) were −100 mV and 10 ms. According to the results of Brown, Lee, and Powell (1981) and Benndorf and Nilius (1987), this should allow Na channels 50–80% recovery from inactivation. We believe that our choice of parameters gives a more reliable estimate, provided that we add ≃1 nC/μF to the component inactivated at more negative voltages (to correct for the use of a relatively depolarized gap voltage, as discussed in Results).

A conclusion from these studies is that Na channel gating current represents a relatively small fraction (25%) of the total charge observed in guinea pig ventricular myocytes. Previous studies (Bean and Ríos, 1989; Hadley and Lederer, 1989, 1991) and our present results provide evidence that the remaining charge is associated with Ca channel gating. Thus, even without resorting to depolarized holding potentials, the properties of total charge, and especially of the portion that activates beyond −70 mV, should largely reflect those of Ca gating charge.

L-Type Ca Channel Gating Current and DHP Binding Densities

Our estimate of Ca gating charge, 10.5–11 nC/μF, is somewhat higher than previous values (Bean and Ríos, 1989; Hadley and Lederer, 1989, 1991). This figure should be compared with current estimates of density of DHP receptors, which range in adult mammalian species from 200 to 1,300 fmol/mg of membrane protein (Kazazoglou, Schmid, Renaud, and Lazdunski, 1983; Doyle, Kamp, Palfrey, Miller, and Page,

1986). Using 1 or 2 × 10^{-10} mg membrane protein/μm^2 (this figure will be justified in the next section) the calculated density of DHP receptors ranges from 12 to 156 molecules/μm^2. To account for 10.5 nC/μF, which corresponds to 656 elementary charges/μm^2 (if the linear membrane capacitance is 1 $\mu F/cm^2$), it is necessary to assume from 4 to 55 elementary charges moving across the field per molecule, depending on the figure used for DHP receptor density.

The density of low affinity tetrodotoxin (TTX) binding sites in mammalian cardiac muscle is ≃500 fmol/mg membrane protein (Renaud, Kazazoglou, Lombert, Chicheportiche, Jaimovich, Romey, and Lazdunski, 1983; Doyle et al., 1986). This is two- to threefold lower than the estimates of DHP receptor density from the same authors (Doyle et al., 1986). From these figures the ratio of gating charge should be between 2 and 3 if Ca and Na channels have similar charge transfer per channel. Our present measurements give a ratio of 3 (10.5/3.5), and are thus consistent with similar charge transfer in Na and Ca channel gating.

Even though the amount of charge attributed here to Ca channels is threefold higher than the corresponding estimate in neonatal rat myocytes (Field et al., 1988) the greater amount is entirely consistent with the increase in DHP binding capacity reported for the first week after birth in rat and chick hearts (Kazazoglou et al., 1983; Renaud, Kazazoglou, Schmid, Romey, and Lazdunski, 1984).

Correlation of Na Channel Gating and Ionic Current Densities

As with Ca channels, the density of Na channels may be estimated from biophysical considerations (the steepness of the activation curves for ionic current and charge movement) and from biochemical measurements of specific toxin-binding sites. In single rat ventricular myocytes (Brown et al., 1981) the voltage dependence of activation of Na ionic current has a steepness factor of 6 mV at 20–22°C, implying a minimum transfer of 4 e per channel. The steepness factor of charge movement in our experiments is K_{Na} = 9.6 (2.1) mV, which corresponds to at least 2.5 e per voltage sensor. The corresponding number for the charge movement of canine Purkinje cells (Hanck et al., 1990), which apparently arises almost entirely from Na channels, is 10.8 mV. Thus the existing measurements are consistent with transfer of charge in independent quanta of 2–2.5 e, and higher transfer for channel opening. This discrepancy can be reconciled, invoking multiple particle gating of individual channels.

A charge transfer of 3.5 nC/μF corresponds to 218 $e/\mu m^2$, or 87 independently moving particles of 2.5 e per μm^2. The density of channels has been estimated by Bean and Ríos (1989) and Hadley and Lederer (1989) from published ionic current measurements at 25–50/μm^2. Again, the estimates from gating current and ionic current are consistent only if multiple voltage sensing particles are involved in gating of individual channels.

Two types of TTX binding sites are experimentally detected, of which only the low affinity sites may be functional channels (Renaud et al., 1983). The density of these sites is 400–600 fmol/mg membrane protein, or 2.4–3.2 × 10^{11} sites/mg membrane protein. From this and the estimate of channel density per unit area (25–50/μm^2) a figure can be derived for the density of membrane protein, 1 or 2 × 10^{-10} mg/μm^2. This figure was used in the previous section to estimate density of Ca channels.

The Slow Component of Charge Movement Arises from Inactivated Channels

The existence of a slow OFF gating current with a time constant of ~10 ms was shown by Hadley and Lederer (1989) in guinea pig myocytes. They proposed that it could represent "... remobilization of immobilized charge," that is, transitions of recovery from inactivated states. We propose an alternative interpretation of this slow charge movement, and show below that it is consistent with all its attributes, described in this and previous papers.

The component only appears after substantial depolarization, it is distributed over a very negative voltage range, and its kinetics depend on repolarization voltage only, with a time constant that peaks at 12 ms at voltages near −100 mV. These properties are similar to those of charge 2 in skeletal muscle (Adrian and Almers, 1976; Brum and Ríos, 1987).

As it was proposed for charge 2 in skeletal muscle, there is every indication in cardiac muscle that its appearance is due to voltage-dependent inactivation (of Ca channels, as these are the source of most of the charge) and reflects the change in voltage dependence and kinetics of Ca gating charge associated with inactivation of the channels.

Three main properties associate the appearance of slow charge with Ca channel inactivation: (*1*) Slow charge requires prolonged depolarization at potentials that cause inactivation of I_{Ca}. (*2*) Its appearance depends on the duration of the inactivating pulse, exponentially increasing with a time constant of ~500 ms. In experiments of Josephson, Sanche-Chapula, and Brown (1984) in guinea pig ventricular myocytes (at room temperature and at −10 mV), the inactivation of Ba currents through Ca channels followed a two-exponential decay, and the major (slow) component had a time constant of ~160 ms.[4] The Ba currents recorded in the same tissue and under similar conditions by Lee, Marban, and Tsien (1985) relaxed more slowly, with a characteristic time of several hundred milliseconds. (*3*) Slow charge disappears as a function of the interval between conditioning and test pulses with a time constant of 200 ms. Ca currents in guinea pig ventricular myocytes recover from inactivation with time constants of 122 and 433 ms at room temperature (Josephson et al., 1984). Another indication that the appearance of slow charge movement is associated with ion channel inactivation is that its properties are analogous to those of charge 2 in skeletal muscle, where the link with inactivation is well established. Work in progress in our laboratory aims at measuring simultaneously charge 2 and ionic currents in order to refine the above comparisons.

A shift in the voltage dependence of charge movement accompanying voltage-dependent inactivation was first shown for slow inactivation of Na channels in squid axons (Bezanilla, Taylor, and Fernández, 1982). Thus, it is almost certain that part of the charge 2 in the present experiments is contributed by inactivated Na channels, but we do not know how much. Since the maximum Na channel contribution to charge 1 is 25%, the Na channel contribution to charge 2 should not be greater than 25% (and is likely to be less, as the Na channels should recover from inactivation more rapidly than Ca channels during the necessary gaps). Therefore, even though

[4] The fast phase of inactivation, with a time constant of ≈30 ms, is presumably ion dependent and would not operate in the present experiments, in which ionic currents are blocked.

the Na channel contribution is likely to have different kinetics and a different time course of onset and recovery, the properties of charge 2 in guinea pig myocytes should be largely determined by the Ca component.

A State Model of Charge 2 in Cardiac Muscle

The identification of the slow charge in the present experiments with skeletal muscle charge 2 allows us to extrapolate directly the formalism developed in skeletal muscle for its description and interpretation. In skeletal muscle, most of the intramembrane charge (charge 1 as well as charge 2) is thought to be produced by the voltage sensor of E-C coupling, a molecule similar to a Ca channel (Ríos and Brum, 1987; Tanabe, Beam, Powell, and Numa, 1988). Therefore, the skeletal muscle formalism should apply strictly to the portion of intramembrane charge of cardiac muscle corresponding to Ca channels. At present we lack a criterion to separate this component. Since we expect it to be dominant, we will apply the theory to all of the charge measured in the ventricular myocytes.

The theory of charge 2 in skeletal muscle includes a specific minimum state model, initially proposed by Bezanilla et al. (1982) for inactivation of squid axon Na channels and then developed for charge movements of skeletal muscle by Brum and Ríos (1987).

$$\begin{array}{ccc} & Q_2 & \\ I^* & \Leftarrow & I \\ \Downarrow & & \Uparrow \\ R & \Rightarrow & A \\ & Q_1 & \end{array}$$

The four-state model includes a resting state R, an active state A, and two inactivated states. It assumes that the transitions represented horizontally are voltage dependent, generating charge movements, and fast, meaning that the charge movements are measurable, whereas the vertical transitions are slow and voltage independent. All transitions are, of course, reversible, but the arrows point in the preferred direction during an inactivating depolarization–repolarization cycle. When a cell held at the resting potential is depolarized, the voltage sensors go from R to A (which underlies charge 1), and then slowly go into I. Once the system is inactivated, short-term changes in potential will only move the system between I and I*, causing charge 2.

The property of skeletal muscle that made this description possible is the orders-of-magnitude difference between the rates of the vertical (inactivation and repriming) and horizontal transitions. This difference makes the two charges experimentally separable, as the horizontal transitions reach equilibrium at times when the vertical transitions have barely progressed. The appearance of charge 2 in skeletal muscle requires seconds at 0 mV, whereas in cardiac muscle it only requires a depolarization lasting $\simeq 50$ ms to be measurable, and has time constants of onset and recovery in the hundreds of milliseconds. Therefore, the differences in temporal scale of vertical and horizontal transitions is less clear-cut in cardiac muscle.

Note that there is an essential difference between this model and the interpretation of the slow current proposed previously (Hadley and Lederer, 1991) resulting from

channels recovering from immobilization. As discussed earlier for skeletal muscle (Brum and Ríos, 1987) such interpretation amounts to proposing a three-state model

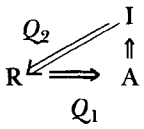

in which the slow charge originates in the I ⇔ R transition. This was ruled out in skeletal muscle, and should be ruled out here, because the movement of slow charge, which takes place in ≈20 ms at −100 mV, is not accompanied by recovery from inactivation. Thus, at least two inactivated states are required, among which charge can move without recovery from inactivation.[5]

A most striking aspect of the results is that the total charge remains at a constant amount, in spite of large changes in charge 1 and charge 2 induced by the conditioning. Since the charge transfer in a complete loop around the four-state diagram should be zero, the experimental equality of charges 1 and 2 requires either that there is no charge associated with the vertical transitions, or that the charge transfer between A and I and between R and I* is identical.

A related observation is that the steepness factors of the Boltzmann distributions describing charge 1 and charge 2 are very similar, more so than in skeletal muscle. This is also consistent with the hypothesis that there is no intrinsic voltage dependence in the vertical transitions (or that the voltage dependence is identical for R ⇔ I* and A ⇔ I). In this view the inactivated voltage sensor still has the same charge and traverses the same fraction of the membrane field upon depolarization, though its equi-distribution voltage has changed. This simple picture puts constraints on the possible molecular models of inactivation. Moreover, it is inconsistent with state models currently in favor for Na channels, like the one shown below, in which several closed states linked by voltage-dependent transitions are outside of the activation–inactivation loops, and therefore contribute to charge 1 (Q_{10}, Q_{11}) but not charge 2.

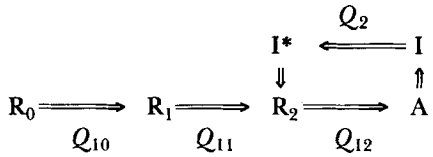

One of the interesting aspects of the four-state model above is that it predicts sigmoidal inactivation with increasing holding potential in the absence of any intrinsic voltage dependence of the inactivation (or recovery) transitions. It can be demonstrated (Brum et al., 1988) that the availability of charge 1 ($Q_a \equiv$ sum of the occupancies of states R and A) depends on the holding potential (V) as follows:

$$Q\mathrm{a} = \{1 + K_i[1 + e^{-(V-\overline{V}_2)/K}]/[1 + e^{-(V-\overline{V}_1)/K}]\}^{-1} \quad (2)$$

[5] As stated above, however, the vertical transitions (inactivation and repriming or recovery) are substantially faster in cardiac channel gating, and it is possible, at least in theory, to detect the charge movement currents associated with these transitions.

where K_i is the (voltage-independent) equilibrium constant of inactivation $P(I)/P(A)$ and $\overline{V}_1$ and $\overline{V}_2$ are the transition voltages of charge 1 and charge 2. The above expression can be put as the sum of a constant plus a Boltzmann function with negative slope:

$$Qa(V) = A + B\,[1 + e^{-(V-\overline{V}_i)/K}] \tag{3}$$

where $\overline{V}_i$, the voltage of half-inactivation, is related to the midpoints of charge 1 and charge 2 by

$$\overline{V}_i/K = \ln \frac{e^{\overline{V}_1/K} + K_i e^{\overline{V}_2/K}}{1 + K_i} \tag{4}$$

implying that $\overline{V}_i$ is a logarithmic mean of $\overline{V}_1$ and $\overline{V}_2$ with weights 1 and K_i. When the intrinsic tendency to inactivation (K_i) is large, the midpoint of inactivation moves close to the midpoint of charge 2.

Application of this formalism to the Ca gating current of cardiac muscle requires evaluating the parameters. $\overline{V}_1$ is $\simeq -25$ mV (average of experiments in Figs. 14 and 15). $\overline{V}_2$ can be taken from Fig. 15 as -99 mV (although the possibility that the distribution obtained after depolarization is not pure charge 2 will be considered later). K_i, the equilibrium constant of the inactivation transition, can be estimated as the reciprocal of the fraction of Ca channel current remaining after a long depolarization, or the reciprocal of the fraction of charge remaining after a long depolarization, in a voltage range where only charge 1 moves. The first estimate can be obtained from published data (Hadley and Hume, 1987) as $K_i = 1.5$. The second estimate can be obtained from our Fig. 7, which shows that a pulse from -70 mV moves ~ 9.5 nC/μF when the conditioning potential is -70 mV and ~ 4 nC/μF at high conditioning potentials. The intrinsic inactivation constant K_i would be $(9.5 - 4)/4$, or 1.4, if it is assumed that all the charge moved by the pulse from -70 mV is charge 1. If, as Fig. 15 suggests, 1 nC/μF of the remaining 4 nC/μF was charge 2, the estimate of K_i would become $(9.5 - 3)/3$, or 2.2. Using 10 mV for the common steepness factor K, the extreme estimates of $\overline{V}_i$ are -33.7 mV (for $K_i = 1.4$) and -36.6 mV ($K_i = 2.2$). From the fit of Fig. 7 the voltage for half-inactivation of Ca gating charge is -34.5 mV, which falls within the narrow range predicted by the theory. In summary, there is no need to assume an intrinsic voltage dependence of the inactivation transitions to explain voltage-dependent inactivation of current or voltage-dependent interconversion of charge.

A slight inconsistency in this analysis is that the relatively small value of K_i predicts an incomplete conversion of charge 1 to charge 2, even at the highest depolarizations. Thus, for $K_i = 2$, only two-thirds of the charge represented by open symbols in Fig. 15 would be charge 2, and the other third would be charge 1. Upon close examination there is an indication of a second Boltzmann component in the depolarized myocyte, centered near -40 mV and involving $\sim 25\%$ of the charge. The coexistence of charges 1 and 2 in this distribution would introduce an error in the estimate of $\overline{V}_2$. Other limitations include the assumption of a single class of inactivated states, which neglects the duality of voltage- and Ca^{2+}-dependent inactivation. The theory is an initial approximation to voltage-dependent inactivation only.

Regardless of the limitations it is clear—and this is one of the main outcomes of the present work—that the simple four-state model of charge movement has substantial value to both the understanding and prediction of the inactivation properties of the Ca channel.

Our results have general implications for understanding the inactivation process of many types of voltage-dependent ionic channels. The term "immobilization" does not describe adequately the effects of inactivation on gating charge. Clearly, charge of Ca channels is not immobilized when the channel inactivates; instead its voltage dependence is shifted to more negative potentials. We showed that the time course of the current associated with these transitions is unrelated to either development of or recovery from inactivation, thus rebutting the concept of charge returning from immobilization, and favoring that of charge moving in transitions between inactivated states. Slow inactivation of Na channels of the squid axon results in a similar interconversion of charge (Bezanilla et al., 1982). Recent work of Bezanilla, Perozo, Papazian, and Stefani (1991) shows a similar phenomenon in *Drosophila* Shaker potassium channels expressed in *Xenopus* oocytes. It is therefore clear that the charge 1 – charge 2 scheme proposed for charge movement and inactivation in skeletal muscle is much more generally applicable.

We are deeply indebted to our co-worker, Dr. Adom González, who was the first to realize that the slow charge movement described here is analogous to charge 2, and who made many additional suggestions.

This work was done during the tenure, by R. Shirokov, of a Research Fellowship of the American Heart Association of Metropolitan Chicago. We were also supported by a grant from the American Heart Association (No. 88661, to E. Ríos) and by NIH grant NS-21111 (to R. Levis).

REFERENCES

Adams, D. J., and P. W. Gage. 1979. Sodium and calcium gating currents in *Aplysia* neuron. *Journal of Physiology.* 291:467–481.

Adrian, R. H., and W. Almers. 1976. Charge movement in the membrane of striated muscle. *Journal of Physiology.* 254:339–360.

Armstrong, C. M. 1981. Sodium channels and gating currents. *Physiological Reviews.* 61:644–683.

Armstrong, C. M., and F. Bezanilla. 1973. Currents related to movements of the gating particles of the sodium channels. *Nature.* 242:459–461.

Bayer, R., D. Kalusche, R. Kaufmann, and R. Mannhold. 1975. Inotropic and electrophysiological actions of verapamil and D 600 in mammalian myocardium. III. Effects of the optical isomers on transmembrane action potentials. *Naunyn-Schmiedeberg's Archives of Pharmacology.* 290:81–97.

Bean, B. P., and E. Ríos. 1989. Nonlinear charge movement in mammalian cardiac ventricular cells. Components from Na and Ca channel gating. *Journal of General Physiology.* 94:65–93.

Benndorf, K., and B. Nilius. 1987. Inactivation of sodium channels in isolated myocardial cells. *European Biophysics Journal.* 15:117–127.

Bezanilla, F., E. Perozo, D. M. Papazian, and E. Stefani. 1991. Molecular basis of gating charge immobilization in Shaker potassium channels. *Science.* 254:679–683.

Bezanilla, F., R. E. Taylor, and J. M. Fernández. 1982. Distribution and kinetics of membrane dielectric polarization. I. Long-term inactivation of gating currents. *Journal of General Physiology.* 79:21–40.

Brown, A. M., K. S. Lee, and T. Powell. 1981. Sodium current in single rat heart muscle cells. *Journal of Physiology.* 318:479–500.

Brum, G., R. Fitts, G. Pizarro, and E. Ríos. 1988. Voltage sensors of the frog skeletal muscle membrane require calcium to function in excitation-contraction coupling. *Journal of Physiology.* 398:475–505.

Brum, G. and E. Ríos. 1987. Intramembrane charge movement in frog skeletal muscle fibers. Properties of charge 2. *Journal of Physiology.* 387:489–517.

Byerly, L., R. Meech, and W. Moody, Jr. 1984. Rapidly activating hydrogen ion currents in perfused neurons of the snail *Lymnea Stagnalis*. *Journal of Physiology.* 351:199–216.

Caputo, C., and P. Bolaños. 1989. Effects of D-600 on intramembrane charge movement of polarized and depolarized frog muscle fibers. *Journal of General Physiology.* 94:43–64.

Doyle, D. D., T. J. Kamp, H. C. Palfrey, R. J. Miller, and E. Page. 1986. Separation of cardiac plasmalemma into cell surface and T-tubular components. Distribution of saxitoxin- and nitrendipine-binding sites. *The Journal of Biological Chemistry.* 261:6556–6563.

Fawcett, D. W., and N. T. McNutt. 1969. The ultrastructure of the cat myocardium. *Journal of Cell Biology.* 42:1–45.

Feldmeyer, D., W. Melzer, and B. Pohl. 1990. Effects of gallopamil on calcium releases and intramembrane charge movements in frog skeletal muscle fibres. *Journal of Physiology.* 421:343–362.

Field, A. C., C. Hill, and G. D. Lamb. 1988. Asymmetric charge movement and calcium currents in ventricular myocytes of neonatal rat. *Journal of Physiology.* 406:277–297.

Hardley, R. W. and J. R. Hume. 1987. An intrinsic potential-dependent inactivation mechanism associated with calcium channels in guinea pig myocytes. *Journal of Physiology.* 389:205–222.

Hadley, R. W. and W. J. Lederer. 1989. Intramembrane charge movement in guinea-pig and rat ventricular myocytes. *Journal of Physiology.* 415:601–624.

Hadley, R. W. and W. J. Lederer. 1991. Properties of L-type calcium channel gating current in isolated guinea pig ventricular myocytes. *Journal of General Physiology.* 98:265–285.

Hamill, O. P., A. Marty, E. Neher, B. Sakmann, and F. J. Sigworth. 1981. Improved patch-clamp techniques for high-resolution current recording from cells and cell-free membrane patches. *Pflügers Archiv.* 391:85–100.

Hanck, D. A., M. F. Sheets, and H. A. Fozzard. 1990. Gating current associated with Na channels in canine cardiac Purkinje cells. *Journal of General Physiology.* 95:439–457.

Hui, C. S., R. L. Milton, and R. S. Eisenberg. 1984. Charge movement in skeletal muscle fibers paralyzed by the calcium-entry bloker D-600. *Proceedings of the National Academy of Sciences, USA.* 81:2582–2585.

Isenberg, G., and U. Klöckner. 1982. Calcium tolerant ventricular myocytes prepared by preincubation in a "KB-medium." *Pfügers Archiv.* 395:6–18.

Josephson, I. R., J. Sanches-Chapula, and A. M. Brown. 1984. A comparison of calcium currents in rat and guinea pig single ventricular cells. *Circulation Research.* 54:144–156.

Kazazoglou, T., A. Schmid, J. F. Renaud, and M. Lazdunski. 1983. Ontogenic appearance of Ca^{2+} channels characterised as a binding sites for nitredipine during development of nervous, skeletal and cardiac muscle systems in the rat. *FEBS Letters.* 164:75–79.

Keynes, R. D., and E. Rojas. 1974. Kinetics and steady-state properties of the charged system controlling sodium conductance in the squid giant axon. *Journal of Physiology.* 239:393–434.

Kostyuk, P. G., O. A. Krishtal, and V. I. Pidoplichko. 1977. Asymmetrical displacement currents in nerve cell membrane and effect of internal fluoride. *Nature.* 267:70–72.

Lee, K. S., E. Marban, and R. W. Tsien. 1985. Inactivation of calcium channels in mammalian heart cells: joint dependence on membrane potential and intracellular calcium. *Journal of Physiology.* 364:395–411.

Legato, M. J., and G. A. Langer. 1969. The subcellular localization of calcium ion in mammalian myocardium. *Journal of Cell Biology.* 41:401–423.

Pizarro, G., R. Fitts, M. Rodriguez, I. Uribe, and E. Ríos. 1988. The voltage sensor of skeletal muscle exitation-contraction coupling: a comparison with Ca^{2+} channels. *In* The Calcium Channel: Structure, Function and Implications. M. Morad, W. Nayler, S. Kazda, and M. Schramm, editors. Springer-Verlag, Berlin. 138–158.

Renaud, J. F., T. Kazazoglou, A. Lombert, R. Chicheportiche, E. Jaimovich, G. Romey, and M. Lazdunski. 1983. The Na^+ channel in mammalian cardiac cells. *The Journal of Biological Chemistry.* 258:8799–8805.

Renaud, J. F., T. Kazazoglou, A. Schmid, G. Romey, and M. Lazdunski. 1984. Differentiation of receptor sites for [^{3}H]nitrendipine in chick hearts and physiological relation to the slow Ca^{2+} channel and to excitation-contraction coupling. *European Journal of Biochemistry.* 139:673–681.

Ríos, E., and G. Brum. 1987. Involvement of dihydropyridine receptors in excitation-contraction coupling in skeletal muscle. *Nature.* 325:717–720.

Ríos, E., and G. Pizarro. 1991. The voltage sensor of excitation-contraction coupling in skeletal muscle. *Physiological Reviews.* 71:849–908.

Schneider, F. M. and W. K. Chandler. 1973. Voltage dependent charge movement in skeletal muscle: a possible step in exitation-contraction coupling. *Nature.* 242:244–246.

Shirokov, R., R. Levis, N. Shirokova, and E. Ríos. 1992. Two classes of gating current from L-type Ca-channels in guinea pig ventricular myocytes. *Biophysical Journal.* 61:A408.

Tanabe, T., K. G. Beam, J. A. Powell, and S. Numa. 1988. Restoration of excitation contraction coupling and slow calcium current in dysgenic muscle by dihydropyridine receptor complementary DNA. *Nature.* 336:134–139.